

Unsupervised Doppler Radar-Based Activity Recognition for e-healthcare

Yordanka Karayaneva¹, Sara Sharifzadeh¹, Wenda Li², Yanguo Jing¹,
Bo Tan³

¹Faculty of Engineering, Environment and Computing, Coventry University, UK (e-mail: (karayany,ac8115,ac2716)@coventry.ac.uk)

²University College London, UK (email:wenda.li@ucl.ac.uk)

³Tampere University, Finland (email: bo.tan@tuni.fi)

May 16, 2022

Abstract

Passive radio frequency (RF) sensing and monitoring of human daily activities in elderly care homes has recently become an emerging topic due to the demand with ageing population. Micro-Doppler radars are an appealing solution considering their non-intrusiveness, deep penetration, and high-distance range. This study presents an unsupervised framework for human activity monitoring using Doppler streams. Two unsupervised feature extraction strategies based on convolutional filtering and texture analysis of Doppler images are considered. For the former, encoded features using Convolutional Variational Autoencoder (CVAE) are compared with Convolutional Autoencoder (CAE) features. For the latter, Grey-Level Co-occurrence Matrix (GLCM) is used. These methods are further compared with unsupervised linear feature extraction based on Principal Component Analysis (PCA) and Singular Value Decomposition (SVD). Using these features, unsupervised samples clustering is performed using K-Means and K-Medoids. Actual labels are solely used for evaluation and visualisation. The results showcase 82.5% and 84% average testing accuracies for CVAE features and 77.5% and 72.5% average testing accuracy using texture features based on GLCM using K-Means and K-Medoids respectively. The results show superiority of CVAE and GLCM features compared to PCA, SVD, and CAE with more than 20% average accuracy. Furthermore, for high-dimensional data visualisation, three manifold learning techniques are considered including t-Distributed Stochastic Neighbour Embedding (t-SNE), Multidimensional Scaling (MDS), and Locally Linear Embedding (LLE). The visualisation methods are compared for projection of raw data as well as the encoded features using CVAE. All three methods show an improved visualisation ability when applied on the transformed CVAE data.

Index terms— Activity recognition, Data visualization, Doppler radar, Health and safety, Unsupervised learning.

1 Introduction

Human activity recognition for smart healthcare is an emerging topic. It is becoming even more prominent with the complications of ageing population worldwide. The population aged 65+ in the UK was 11.8 million in 2016, while this number is projected to grow to 20.4 million by 2041 [1]. Chronic and long-term conditions are well-known to increase with age. It is reported that 29% of those aged 60-64 had a chronic condition, while the percentage grows to 50% for elderly populations aged 75 or over. The implications of ageing with chronic conditions prevent elderly people from independent living. Thus, they are dependent on social care services such as living in care homes.

The demand for human activity detection and monitoring has rapidly increased over the past years. A number of devices are proposed including cameras, wearable technologies, infrared sensors, and radars. These devices are expected to provide daily monitoring of elderly people's activities and vital signs. Hence, this will provide peace of mind for their relatives regarding the physical health and mental health of the care home residents. Cameras are often seen as an obvious and traditional solution for capturing observable data including human activities for subsequent recognition [2], [3] [4]. Video-depth cameras are capable of obtaining extremely high-resolution data, which can contribute to the detailed analysis of daily human activities. Nevertheless, camera devices suffer from intrusiveness, which is highly undesirable in the contexts of residential environment. The modern healthcare is concerned with the privacy and dignity of patients. Therefore, vision-based solutions are not recommended in smart care homes.

Wearable sensor technologies are an effective solution for smart healthcare applications as they provide a combination of human activity recognition and vital signs detection [5], [6], [7], [8]. Despite their existence since the 1960s, wearable sensors have become common in people's daily lives in the recent years with the increasing popularity of commercial smart watches. Wearable sensors have the ability to capture small fractions of the body such as the movement of elbows, knees and even fingers [9]. Additionally, wearable sensing technologies can detect physiological signals such as heart rate and speech patterns [10]. However, the disadvantages and challenges of this technology are not to be underrated. Wearable sensors are known to have poor battery life [11]. As they are "wearable", elderly populations may easily forget to wear the device or feel uncomfortable wearing it [12].

Infrared sensors utilize human's body temperature distinguished from the lower ambient temperature in order to capture and detect human activities. Most IR sensors obtain ultra low-resolution data, where a subject identification is avoided. Thus, IR devices represent an attractive solution to be deployed in care homes and hospitals. Current studies reveal significant recognition rates (>90%) for activities including standing, sitting, walking, falling, and others [13], [14], [15]. Contrarily to their advantages, IR devices suffer from a relatively low detection distance. It has been shown in a recent paper [16] that the performance drops with distance growth although not as significantly. As IR sensors are low-

resolution capturing devices, they lack sensitivity towards small fractions of the human body, which prevents more specific activities detection.

Micro-Doppler radars are a appealing solution for human activity recognition due to their non-intrusiveness, high distance range, deep penetration, and reliable accuracy rates [17], [18] [19]. They are known to have applications in human activity recognition [20], vital signs monitoring such as heart rate and breathing [21], gait patterns analysis [22] and distinguishing emotions [23]. The phenomenon known as Doppler effect can be generated by activities involving motion such as walking, jumping and running, which cause a shift in the frequency. Therefore, the Doppler effect can be used to classify these activities. Micro-Doppler radars have been extensively used for activity recognition with focus on healthcare purposes [21], [24], [25]. Currently, majority studies fall in supervised learning using conventional feature extraction methods as PCA and SVD. In terms of classification of the extracted variance-maximized components, SVM and k-NN are commonly utilised [26]. Deep learning approaches have been recently proposed and Convolutional Neural Networks (CNNs) and Recurrent Neural Networks (RNNs) architectures have been built. Unsupervised learning is yet a minimally research topic for Doppler-radar based applications. The pilot study using the *Doppler-Radar-UCL* dataset [24] considers an unsupervised scenario despite labels availability. The importance of the designed framework is the applicability to projects with poor labeling scenarios. Differently from other approaches, the authors use Hidden Markov Models (HMM) in order to extract activity information from each Doppler sequence. The output of the HMM training in the next step is a log-likelihood matrix, which is clustered using K-Means and K-Medoids. The original log-likelihood presents the similarities between the Doppler sequence and the HMM. Subsequently, three newly derived log-likelihood matrices are proposed, which aim to symmetrize the initial matrix. Accuracy reveals that the Kullback-Leibler (KL) log-likelihood with K-Medoids for clustering obtains the highest accuracy. In previous work [27], unsupervised physical features extraction and classification with HMM is proposed where the achieved accuracy is 72%. The researchers in [20] build a Convolutional Autoencoder (CAE) for unsupervised pre-training for classifying 12 daily activities. Then activity classification was performed based on a supervised framework by fine-tuning and a softmax classifier.

This project manipulates the *Doppler-Radar-UCL* database and proposes an unsupervised framework. Two groups of unsupervised strategies are considered; (1) The convolutional filtering strategies based on CVAE and CAE (2) the texture-based analysis based on GLCM. The extracted features are clustered into different activity groups based on unsupervised clustering strategies using K-Means and K-Medoids. In order to evaluate the results, the known labels are utilised only at result evaluation step. Accuracy rates for the proposed framework with CVAE showcase reasonable average testing rates for K-Means over five random train/test splits, while the K-Medoids performance is slightly higher. In regards to the GLCM-based framework, the accuracy rates for K-Means is higher in comparison with K-Medoids. The proposed framework can be used in projects with poor labeling scenarios. The contributions of the study to the research community are the following:

- **Novel unsupervised framework for Doppler radar data:** This work is a pioneering study concerning unsupervised learning for Doppler-radar

data. The number of classes/groups estimation is comprehensively studied. A broad number of measures are applied including Elbow test, Silhouette analysis, Davies index, and Dunn index. In addition, this study presents two architectures for feature extraction in an unsupervised scenario, which have not been applied previously for Doppler radar-based activity recognition. The first architecture considers a deep CVAE for filtering-based feature extraction, while the second scenario is concerned with GLCM for texture feature extraction. The extracted features are clustered with K-Means and K-Medoids. Both approaches achieve around 20-25% higher average testing accuracy in comparison with features extracted using CAE, PCA, and SVD. The proposed framework can be useful for unsupervised cases or semi-supervised cases with poor labeling.

- **High-dimensional data visualisation enhancement:** Manifold learning methods for high-dimensional data visualisation are considered in this study. Radar Doppler dataset can benefit in regards to activities illustration, which can reveal similarities between certain activity groups. The manifold learning methods are known to provide good separation between the classes [28]. While CVAE encoded data has been used for data visualisation improvement, this study is the first concerned with Doppler radar-based data. The overall goal in this research is to test the manifold learning methods' performance over raw data and encoded data using CVAE to illustrate any improvement for the sake of visualisation. The three methods for high-dimensional data visualisation t-SNE, MDS and LLE are compared in the two scenarios. Initially, the methods are used to transform the raw data $D_{n \times 6400}$ to a 2-dimensional space. Secondly, the transformation is performed on the encoded features by CVAE data $D_{n \times 200}$. The comparison results reveal better separations of the clusters using the three methods when CVAE encoding is used. This showcases the strength of CVAE for data separation. Hence, CVAE encoded features can be used in manifold learning for visualisation purposes.

The rest of the paper is organized as follows: In Section 2 the methods including the database description, number of clusters estimation and the proposed approaches for feature extraction and clustering are described. Additionally, three methods for data visualisation are defined. The results are shown in Section 3. Then, data visualisation techniques are compared using the raw data transformation and CVAE encoded data. Section 4 critically evaluates the main findings of the study, including the two proposed architectures for unsupervised learning and the manifold learning methods for high-dimensional data visualisation. Finally, Section 5 concludes the study with the most valuable outcomes.

2 Methodology

This study's framework consists of a number of steps illustrated in Figure 1. Initially, the raw dataset's dimensions are manipulated and the dataset is divided into training and testing. The number clusters K is estimated with four metrics. Then, two models are created with the two proposed methods for feature extraction: 1) deep CVAE, and 2) GLCM. Clustering and recognition is achieved with K-Means and K-Medoids. Comparison of the two models is

performed with PCA, SVD and CAE for raw data feature extraction followed by clustering with K-Means and K-Medoids. The following paragraphs outline the dataset description, feature extraction methods, clustering techniques, and visualisation methods.

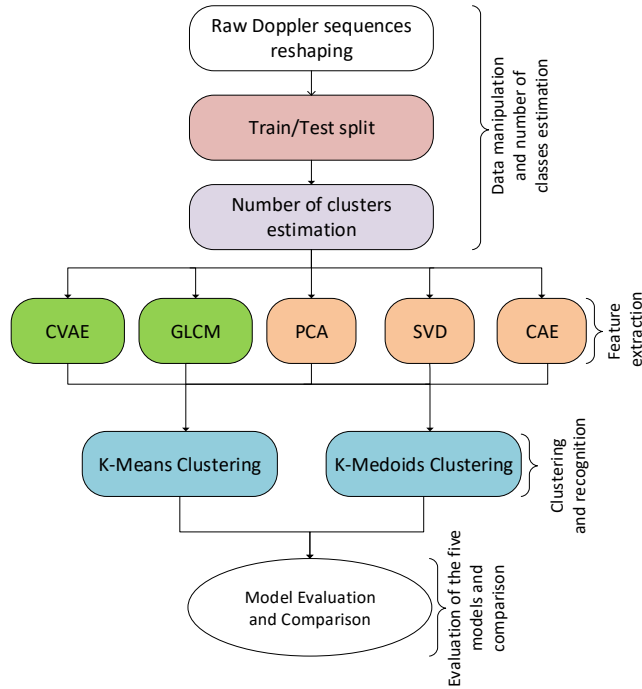


Figure 1: Project flowchart

2.1 Dataset Description

The Doppler-sequences were collected in the University of Bristol laboratory using the energy harvesting transmitter TX91501 POWERCASTER as the signal source. The passive radar sensors consists of two channels: 1) surveillance channel for capturing the reflected signal; and 2) reference channel, which receives the transmitted signal. The signal source is located 0.5 m from the source. Four participants (one female and three male) were used for capturing activities. Figure 2 illustrates the experimental $7\text{ m} \times 5\text{ m}$ layout for the RF dataset. This dataset consists of five activities: (1) Walking, (2) Running, (3) Jumping, (4) Turning, and (5) Standing. Each activity is repeated 10 times by each subject. There exist 40 samples for each activity or 200 samples totally.

A pre-processed dataset is used in this study. The total number of features per sample is $6400 = (2\text{ directions} \times 100\text{ Doppler bins} \times 32\text{ time index})$. Furthermore, the data is normalized, which corresponds to the fact that all features are represented by real values in the range of $(0, 1)$. Considering the 3-dimensionality of the data, it is then vectoried $2 \times 100 \times 32$, which results in 6400. In order to transform it to a 2D representation, 80×80 reshaping

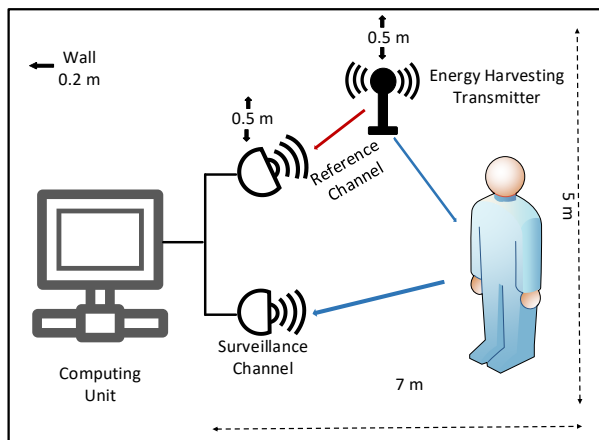


Figure 2: Experimental layout

is applied. An example of each activity in a 2D representation can be seen in Figure 3.

The Python libraries used for data pre-processing are pandas (version 1.0.5) and numpy (version 1.19.1). In terms of machine learning for feature extraction and clustering, scikit-learn (version 0.22.2) and scikit-learn-extra (version 0.1.0b2) modules are applied. The CAE and CVAE are implemented and run with Keras (version 2.2.4) and Tensorflow (version 2.2.0). The visualisation results are implemented with matplotlib (version 3.2.2).

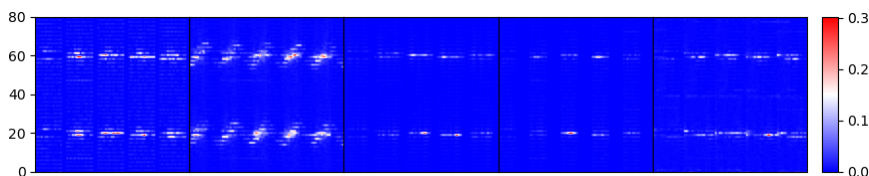


Figure 3: Example of an $80 \times 80 = 6400$ image for each activity: (1) Walking, (2) Running, (3) Jumping, (4) Turning, and (5) Standing

2.2 Number of classes estimation

Considering the unsupervised scenario in this study, the number of classes/clusters is unknown. In order to estimate the correct number, a number of techniques are applied including Elbow method, Silhouette analysis, Davies score and Dunn score using K-Means clustering.

2.2.1 Elbow method

The Elbow method is a heuristic technique for clusters number estimation [29], [30]. The overall goal for the method is to maximize the inter-class variability and minimize the intra-class variability. In this study, the data samples are denoted as $D = D_1, D_2, \dots, D_n$. The number of clusters is K and their centroids

are given by $\omega_1, \omega_2, \dots, \omega_K$. The distortion J is used to measure the effectiveness of the method:

$$J(K, \omega) = \frac{1}{n} \sum_{i=1}^n (\min_{j=1}^K (D_i - \omega_j)^2) \quad (1)$$

In this study, the candidate numbers of clusters $K = 2, 3, \dots, 10$ are selected for K-Means clustering, which is described later in this section. The Elbow method computes the sum of squared errors for the data samples in each cluster. As the number of clusters increases, J becomes smaller. However, the best value of J is the point, where further increase to the number of clusters does not change the within-cluster sum of squares significantly. However, a further increase would result in over-clustering. The decrease trend of J is noticeable before reaching the actual number of clusters K and becomes smoother afterwards. The Elbow method is a visualisation tool, and the graph shows a noticeable decline when the curve approaches the actual K . Therefore, the decline becomes smoother after exceeding K . Figure 4 illustrates the Elbow test for this data. As it can

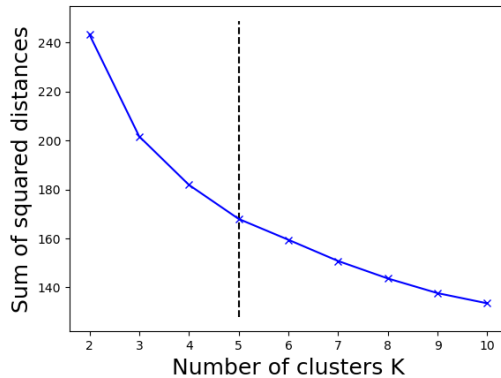


Figure 4: An Elbow test used to determine the number of clusters K

be observed, the selected number of clusters $K = 5$, which is the actual number of clusters for this study. However, detection of this bend point is ambiguous in some cases. Therefore, additional techniques are considered in this study.

2.2.2 Silhouette analysis

Silhouette analysis is one of the most commonly used techniques for number of clusters estimation [31]. The method is given as:

$$Silhouette = \frac{1}{n} \sum_{i=1}^n \frac{b(D_i) - a(D_i)}{\max\{a(D_i), b(D_i)\}} \quad (2)$$

where $a(D_i)$ is the average distance between data point D_i and the remaining data points in its own cluster. The minimum average distance between data point D_i and all other clusters is denoted with $b(D_i)$. The Silhouette coefficient aims to show the suitability for data point D_i to belong to a particular cluster. The score is within the range of $(-1, 1)$, where a lower value refers to overlapping clusters. On the other hand, a higher value suggests well-separated clusters.

2.2.3 Davies-Bouldin index

The Davies-Bouldin index is a clusters estimation method concerned with identifying clusters, which are distinct from each other [32]. The measure is given by:

$$Davies = \frac{1}{K} \sum_{i=1}^K \max_{i \neq j} \frac{\Delta(C_i) + \Delta(C_j)}{\lambda(\omega_i, \omega_j)} \quad (3)$$

where $\Delta(C_i) = \sum_{D_i \in C_i}^n \|D_i - \omega_i\|^2$, which is the distance between each Doppler sequence and the centroid of the corresponding cluster. The distance between cluster centroids is given by $\lambda(\omega_i, \omega_j) = \|\omega_i - \omega_j\|^2$. Then, the term for maximization is computing the ratio of within-cluster to between-cluster distances for the i^{th} and the j^{th} clusters. This is computed for all combinations of cluster i and other clusters. Then, the maximum value is found for each i . Among all combinations of clusters, the closest clusters with largest spreads have the maximum ration. That is the worst scenario. The desire is to minimize the overall average of the worst scenario ratios. Therefore, unlike previous methods, a smaller value for Davies index is desirable.

2.2.4 Dunn index

Dunn index is one of the most popular and oldest techniques in the literature [33]. The overall aim is to minimize the intra-cluster distance and maximize the inter-cluster distance. It is given by:

$$Dunn = \frac{\min_{1 \leq i < j \leq K} \lambda(\omega_i, \omega_j)}{\max_{1 \leq k \leq K} \Delta(C_k)} \quad (4)$$

where $\lambda(\omega_i, \omega_j)$ is the distance between clusters C_i and C_j . The intra-cluster distance of a single cluster is given by $\Delta(C_k)$. The minimization in the numerator finds the Euclidean distance of the two closest clusters. On the other hand, the maximisation in the denominator, finds the Euclidean distance of the samples to the centroid of the cluster with highest dispersion. Therefore, for optimum cluster number, the numerator will be the maximum value among all other candidate number of clusters, while the denominator will be the lowest, resulting a peak over the heuristic search.

Similarly to the Elbow method implementation, a candidate set clusters is given $K = 2, 3, \dots, 10$ for K-Means. The heatmap in Figure 5 shows the results for each heuristic technique. It is important to note that the value for the inverse of Davies index is used. Hence, the highest values corresponding to the darkest colors show the best fit for the clusters. The selected number of clusters is $K = 5$ for all methods.

2.3 Feature extraction methods

In this section, the three main categories of unsupervised feature extraction techniques, convolutional filter-based, texture-based and variation-based projection will be explained.

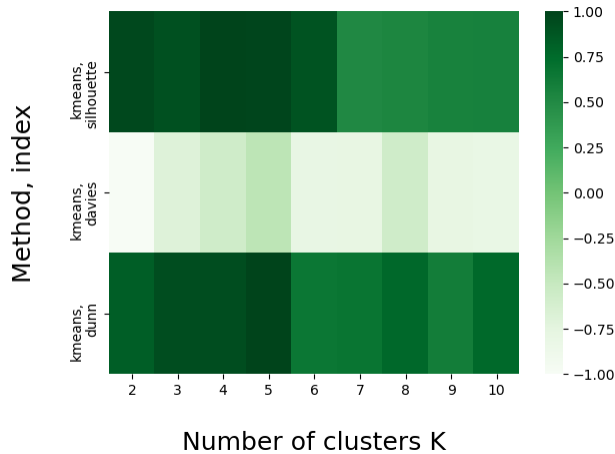


Figure 5: Silhouette score, Davies score and Dunn score used to determine the number of clusters K

2.3.1 Convolution filter-based methods

In this section, a description of CAE is provided by considering its drawbacks. Then, CVAE is introduced, which overcomes the drawbacks of the previous architecture.

Convolutional Autoencoder (CAE) Autoencoders (AEs) are unsupervised neural networks, which can be used for feature extraction. Their architecture consists of two components: an encoder and a decoder [34]. AEs are commonly used for data denoising [35], anomaly detection [36] and image generation [37]. The encoder learns the latent attributes of the input data x and transforms it to a lower dimensionality representation z . On the other hand, the decoder aims to reconstruct x given z . The implementation of CAE only contains a reconstruction loss, which needs to be minimized.

In regards to disadvantages of the discussed architecture, the CAE learns local parameters for each data point. This avoids any statistical strength to be shared across all data points. Hence, this may result in overfitting due to the inability of the model to generalise. In addition, the CAE architecture includes only a reconstruction loss and it lacks any regularisation term as seen in VAEs. This leads to data points of the same group/class to be given different representations, which are often meaningless.

In this work, a deep CAE is used with two hidden layers for the encoder and decoder as illustrated in Figure 6. The retained number of latent variables is 64.

Variational Autoencoder Variational autoencoders (VAEs) are generative models defined in [38], which are commonly used for dimensionality reduction [39], data augmentation [40], and reinforcement learning [41]. VAEs contain two main modules: an encoder, referred to as recognition model or inference model, and a decoder, also defined as generative model [42]. The purpose of

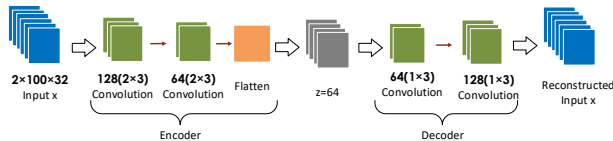


Figure 6: The convolutional AE architecture

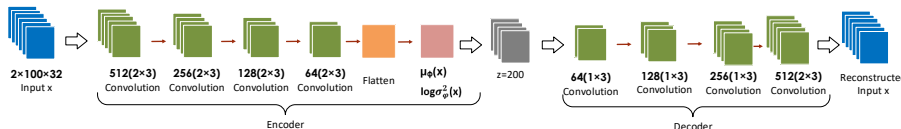


Figure 7: The convolutional VAE architecture

the encoder is to learn the stochastic mappings of the observed input space x with a rather complicated distribution and transform it from its original high-dimensional space (6400 dimensions in this case) into a much lower latent representation z with a relatively simple distribution. Then, the output of the recognition model z is the input of the decoder. The decoder aims to reconstruct the original input x from the reduced latent information. In a traditional autoencoder, the latent representation consist of single-valued outputs for each feature. VAEs assume that the dimensions of z cannot be interpreted with simple variables. Instead, VAEs introduce a probability distribution for the samples of z , which is commonly a Gaussian distribution [43]. The use of a single reconstruction error in encoder-decoders might result in encoding some meaningless content. That results in overfitting and therefore the latent space should be regularised. Contrarily to CAE, in the VAE architecture, the loss function includes a reconstruction term and a "regularisation" term. The latter term is developed by enforcing the probabilistic distribution of the encoded space to be close to a Standard Normal distribution. This is expressed as the Kullback-Leibler (KL) divergence. The KL divergence quantifies the divergence of the latent space distribution, denoted as $q_\theta(z|x)$ in equation 5 and the standard normal distribution $p(z)$:

$$l_i = -E_{z \sim q_\theta(z|x_i)}[\log p_\phi(x_i|z)] + KL(q_\theta(z|x_i)||p(z)) \quad (5)$$

where $p_\phi(x_i|z)$ describes the generative probability of the reconstructed output given the encoded variable z . The distribution of the encoded variable z given the input x_i is denoted as $q_\theta(z|x_i)$. In addition, θ and ϕ are parameters of the distribution.

In this study, four convolutional layers are used for the encoder and the decoder as illustrated in Figure 7. The original high-dimensional data with 6400 variables is transformed to 200 variables of latent representation. The μ_ϕ and $\log \sigma_\phi^2 x$ are the mean and the log variance of the distribution in the encoder.

2.3.2 Texture-based methods

Grey Level Co-occurrence Matrix (GLCM) GLCM is a texture analysis method used for dimensionality reduction [44]. It has been used previously in fall detection application with Doppler-radar [45]. This analysis method

considers the local spatial relationship of pixels with certain intensities and their frequency of occurrences in the image. For instance, it determines the frequencies of occurrences of pixels with gray level G_a to another pixel with gray level G_b at distance d . Thus, GLCM creates a statistical matrix, where the quantifying image texture is shown in Figure 8.

In this study, the dataset is 3-dimensional ($2 \times 100 \times 32$), which is vectorised to 6400 dimensions. In order to convert it to a 2-dimensional data, an 80×80 reshaping is applied. The resulting image is split into local patches of size 10×80 to extract texture features. Then GLCM matrix is formed for two different distances d (one and three number of pixels) and three different angles (0° , 45° and 90°). Therefore, $8 \times 2 \times 3$ GLCM matrices are formed. After forming the GLCM matrices, four different statistics, as shown in equation 6 are computed for each GLCM matrix. Given $8 \times 2 \times 3 = 48$ GLCM matrices, $48 \times 4 = 192$ texture features are extracted from each sample image, resulting an output matrix of size $Z_{n \times 192}$.

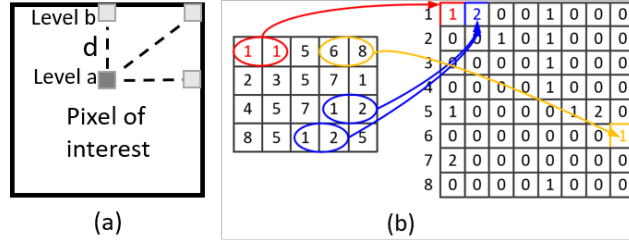


Figure 8: (a) forming the GLCM matrix with three angles 0° , 45° , 90° and (b) Computation of GLCM matrix based on horizontal occurrences at $d=1$ for an image.

The statistics derived in this work are Correlation, Contrast, Dissimilarity, and Energy as described in equation 6:

$$\begin{aligned}
 \text{Correlation} &= \sum_{u,v} |u - v|^2 p(u, v) \\
 \text{Contrast} &= \sum_{u,v} \frac{(u - \omega_u)(v - \omega_v) p(u, v)}{\delta_u \delta_v} \\
 \text{Dissimilarity} &= \sum_{u,v} p(u, v)^2 \\
 \text{Energy} &= \sum_{u,v} \frac{p(u, v)}{1 + |u - v|}
 \end{aligned} \tag{6}$$

where u, v are the row and column indices of the GLCM matrix p . The means and standard deviations are denoted as μ and δ .

2.3.3 Variation-based projection techniques

Principal Components Analysis (PCA) PCA is known to be one of the most common linear techniques for unsupervised feature extraction [46]. This method aims to reduce the dimensionality of data by projecting it into a lower

dimensional space. That is performed by calculating the main directions of variations of data. For this aim, Eigen decomposition of the data covariance matrix $V_{m \times m}$ is obtained, where the highest eigenvalue λ_1 corresponds to the direction of highest variation, w_1 . That is the first Eigen vector. The same way, PCA computes the sorted Eigen values and the corresponding Eigen vectors. In this paper, the s number of the first few Eigen vectors, explaining 95% of data variations, is used to transform the original high dimensional data $D_{n \times m} W_{m \times s} = Z_{n \times s}$.

Singular Value Decomposition (SVD) SVD is a powerful linear technique for feature extraction [47], which decomposes the original matrix $D_{n \times m}$ to:

$$D = UCW^T \quad (7)$$

where $U = n \times n$ representing the left singular values, C is the matrix defined as $n \times m$, and $W = m \times m$ represents the right singular values. The first m components on the diagonal of C , represent the highest standard deviations of the main directions of variations. The off-diagonal components are zero. Finally, using the first few s number of Eigen vectors, corresponding to 0.95 of variations, the data is transformed to a lower dimensional space, $Z_{n \times s} = D_{n \times m} W_{m \times s}$.

2.4 Clustering methods

Two clustering methods are used for grouping the data samples. Both of the methods are distance-based: K-Means and K-Medoids.

2.4.1 K-Means

K-Means clustering is one of the most commonly used techniques for unsupervised learning [48]. The K-Means method considers the number of groups or clusters K is known and it aims to group the data points based on their distances. In this work, the Euclidean distance is used. The overall goal for the clustering method is to group the data points D_1, D_2, \dots, D_n in clusters by minimizing the intra-cluster distances. Intuitively, the distances between data points from different clusters should be maximized. During training, K-Means outputs the cluster centres ω_k , where $k = 1, 2, \dots, K$, or also known as centroids. The assignment of a new data point to one of the clusters is such that, the sum of the squared distances between the data point and all cluster centroids $\omega_1, \omega_2, \dots, \omega_k$ are computed. Then, the sample is assigned to the cluster, where corresponding distance is minimum. The objective function for K-Means, which specifies the sum of squared distances of each data point D_i to cluster k , is defined as follows:

$$J = \sum_{i=1}^n \sum_{k=1}^K r_{ik} \|D_i - \omega_k\|^2 \quad (8)$$

where r_{ik} is a binary function indicating the assignment of data point D_i to cluster k . If D_i is assigned to cluster k , the binary indicator $r_{ik} = 1$, and 0 otherwise:

$$r_{ik} = \begin{cases} 1, & \text{if } k = \arg \min_j \|D_i - \omega_j\|^2 \\ 0, & \text{otherwise} \end{cases} \quad (9)$$

The overall aim is to minimize the J for values r_{ik} and ω_k . The procedure can be achieved by iterative optimization with respect to r_{ik} and ω_k . In the first phase, the ω_k is fixed, while the goal is to optimize r_{ik} . The same notion is applied to the second step as r_{ik} is fixed and the focus is on the optimization of ω_k . The entire process corresponding to Expectation-Maximization algorithm is repeated until convergence.

2.4.2 K-Medoids

K-Medoids is a clustering method based on distances analysis, which is known to be more robust to noises and outliers than K-Means [49]. Similar to K-Means, this method considers the number of groupings or clusters K is known initially and $K < n$, where n is the number of data points. In contrast, K-Medoids considers a data sample for the centroid or the medoid, which is not the case for K-Means. In the first step of K-Medoids, the algorithm aims to find a data point D_i in a cluster $C(i) = k$ that is in minimum distance to the remaining observations in the cluster D'_i . This distance is denoted as $\|D_i - D_{i'}\|^2$ and the minimisation is shown in equation 10:

$$i_k^* = \arg \min_{i:C(i)=k} \sum_{C_{i'}=k}^n \|D_i - D_{i'}\|^2 \quad (10)$$

Then, the output index i_k^* is used to find a new centroid or medoid, defined as $\omega_k = D_{i_k^*}$, $k = 1, 2, \dots, K$ for all clusters.

The second step of the method is to minimise the total error by re-assigning each data sample to the closest centroid. The clusters centroids are given $\omega_1, \omega_2, \dots, \omega_K$.

$$C(i) = \arg \min_{1 \leq k \leq K} \|D_i - \omega_k\|^2 \quad (11)$$

Finally, step 1 and step 2 are iterated until the algorithm converges to the optimum centroids.

2.5 Visualisation techniques for high-dimensional data

In this paragraph, three widely-known techniques for manifold learning are defined. The focus is on transforming the very high-dimensional space in this dataset ($D_{n \times m} = D_{n \times 6400}$) to a 2-dimensional space. Manifold learning methods are known to map closely correlated data samples in similar positions, while the gap in the low dimensional space increases if the samples are non-similar. Hence, comparison measures will be extracted from this analysis, which can be useful for projects concerned about high-dimensional data visualisation.

2.5.1 t-Distributed Stochastic Neighbour Embedding

T-SNE is a non-linear dimensionality reduction method, which has gained attention for its superior ability to visualise high-dimensional data by transforming it to a two or three-dimensional space [50]. This method assigns each data point in a low-dimensional location by aiming to preserve the significance of the original information. Unlike linear techniques such as PCA and SVD, t-SNE aims to

keep similar data points in close locations in the low-dimensional space. The superiority of t-SNE in comparison with other dimensionality reduction methods is the ability to preserve the local structure of the data as well as global information such as clusters. The steps for the t-SNE transformation are described below:

1. The Doppler sequences D_1, D_2, \dots, D_n are initially in their original 6400-dimensional space. T-SNE begins with determining the similarity between the data samples. This is performed by computing their distances. Euclidean distances are used in this study.
2. The Euclidean distances are converted to probabilities describing a normal distributions so that, similar data samples have close values. On the other hand, dissimilar points have distinct similarity values. The similarity scores are calculated for each data points pair D_{ij} , where a similarity matrix is obtained based on probabilities p_{ij} .
3. The data samples are projected in a random order to the low dimensional space first. This results in a mismatch with cluster patterns of data in original domain initially. The aim for t-SNE is to re-position the data samples in the new low dimensional space, such that the same clustering patterns of the high-dimensional space be preserved.
4. Then, the Euclidean distances between the data samples are calculated in the lower dimensional space. Similarly, the distances are converted to a t-Distribution (e.g. q_{ij} for the two data points D_i and D_j). t-Distribution is similar to normal distribution, but with taller tails. The taller tails of t-Distribution prevent dissimilar data points to be positioned in close locations of the lower dimensional space. The samples in lower dimension are re-positioned using these probabilities resembling distances. The re-positioning is performed based on the the two probabilities q of low dimension and p of high dimension.
5. t-SNE uses Kullback-Leibler divergence to optimise the similarity of the distributions described by q to those described by p . This can be interpreted as constant comparison of the samples distances in the lower-dimensional to their distance in the original high-dimension. Then, re-positioning will be improved iteratively, as the similarity matrix of probabilities q is optimized using the original similarity matrix p .

2.5.2 MultiDimensional Scaling (MDS)

MDS is a nonlinear dimensionality reduction technique. It can be used for visualization of high dimensional data in low dimensional space. It preserves the actual distances of original samples in low dimensional space. MDS considers dissimilarities of sample pairs contrary to other methods, which are concerned with similarities. Given the set of observation $D_1, D_2, \dots, D_n \in \mathbb{R}^m$, d_{ij} is the dissimilarities e.g. the Euclidean distance of two samples D_i and D_j so that, $d_{ij} = \|D_i - D_j\|^2$. MDS seeks $z_1, z_2, \dots, z_n \in \mathbb{R}^k$, so that $k < m$. A so called stress function is minimized for this aim [51], [52], [53]:

$$Stress_{(z_1, \dots, z_n)} = \sum_{i \neq j}^n (d_{ij} - \|z_i - z_j\|)^2 \quad (12)$$

where $\|z_i - z_j\|$ is the Euclidean distance between z_i and z_j . Then the pairwise distances are preserved in lower dimensional representation. A gradient descent algorithm is used to minimize the stress function and find the components in low dimension [53]. MDS transformation is monotone increasing with the increasing dissimilarities. The same notion is applied to growing similarities data, which decreases the transformation. Hence, similar object pairs are positioned closely in the transformed space, while objects with dissimilarity are distinguished with larger distances.

2.5.3 Locally Linear Embedding

Locally Linear Embedding (LLE) is a non-linear dimensionality reduction method proposed in [54]. LLE is concerned with preserving the global structure of the data based on an underlying manifold. The data are represented by n real-valued vectors \vec{X}_i in high dimension m . i is the index of a sample. Each data point \vec{X}_i , is a member of a neighbourhood. Each neighbourhood consists of similar data points. Similar data points are expected to lie on a close locally linear patch of the smooth manifold. The p nearest neighbours for each data point are defined by measuring the Euclidean distances. The local geometry of the patches can be characterised by linear coefficients. These linear coefficients are used to reconstruct each data point from its neighbours. The reconstruction loss is defined by:

$$\epsilon(W) = \sum_{i=1}^n \|\vec{X}_i - \sum_{j=1}^p W_{ij} \vec{X}_j\|^2 \quad (13)$$

where W_{ij} are the weights defined for data points reconstruction using the corresponding neighbours. The number of samples is given as n , while the number of neighbours is p . The computed weights W_{ij} correspond to the contribution of data point \vec{X}_j for reconstructing \vec{X}_i . In order to ensure that \vec{X}_i is reconstructed only by its neighbours, the weight function $W_{ij} = 0$, if a sample \vec{X}_j does not belong to the same class. Another constraint to the reconstruction loss is that the sum of the weight matrix's rows should be one, $\sum_{j=1}^p W_{ij} = 1$. This sum-to-one constraint makes the weights invariant to translation of the data points and their neighbors. The weights are also invariant to rotation and scaling. The minimisation of the loss function, allows computation of the weights W . They characterize the intrinsic geometric properties of each neighborhood.

Using the weights, W_{ij} it is possible to project each high-dimensional data point \vec{X}_i to vector \vec{Y}_i of the lower representation based on another reconstruction cost function. Having the W_{ij} fix, the aim is to minimise the embedded cost function to optimise the low d -dimensional coordinates ($d < m$) :

$$\Phi(Y) = \sum_{i=1}^n \|\vec{Y}_i - \sum_{j=1}^n W_{ij} \vec{Y}_j\|^2 \quad (14)$$

3 Evaluation and results

In this section, the results obtained using the three groups of unsupervised feature extraction techniques, including the convolutional filter-based, texture-

based and variational-based projection are presented. For CAE and CVAE, the inputs are n number of 3D cubes of size $2 \times 100 \times 32$. While for PCA and SVD, the input data is $D_n \times 6400$. For GLCM, the inputs are n reshaped images of size 80×80 . In the case of PCA and SVD, the selected number of Eigen vectors preserve 95% of the data variance.

In addition to the activities clustering results, the three manifold learning methods t-SNE, MDS and LLE are compared in two scenarios. In the first scenario, they transform the raw data features to a 2-dimensional space. Since CVAE encoded features obtained the most accurate clustering results, in the second visualization scenario, they are used for projection into a 2-dimensional space.

In all experiments, the dataset is randomly divided into training and testing, where 80% of the data are used for training, and 20% for testing. As the architecture is unsupervised, labels are only used for model evaluation and illustration purposes. The percentage of the clustering accuracy is used for evaluation of the methods.

3.1 Average testing accuracies for K-Means and K-Medoids using all feature extraction techniques

The average training and testing accuracies with standard deviations over five random train/test splits for K-Means and K-Medoids using all feature extraction methods are illustrated in Table 1 and Table 2.

Table 1: Average training accuracies of K-Means and K-Medoids using the five feature extraction methods

	CVAE	GLCM	CAE	PCA	SVD
K-Means	83.02%±7.79	66.87%±0	51.74%±2.85	62.87%±1.88	59.25%±2.03
K-Medoids	79.12%±9.45	69.37%±0	52.99%±3.98	53.62%±6.41	54.12%±2.7

Table 2: Average testing accuracies of K-Means and K-Medoids using the five feature extraction methods

	CVAE	GLCM	CAE	PCA	SVD
K-Means	82.5%±2.73	77.5%±0	53%±1	56%±8.45	57%±9.27
K-Medoids	84%±5.38	72.5%±0	57.5%±9.21	65%±5	55%±6.32

As it can be observed, the two superior architectures are the CVAE encoded features and GLCM texture features. K-Medoids has a better performance than K-Means using the CVAE encoded features. On the other hand, GLCM texture features are better incorporated with K-Means. In addition, PCA and SVD have similar accuracies, while CAE obtains the worst performance.

In order to evaluate their performance for different activity groups, confusion matrices for K-Means and K-Medoids are visualised. The following matrices in Figure 9 consider the CVAE encoded data over different train/test splits for K-Means (Figure 9a) and K-Medoids (Figure 9b).

The confusion matrices for the GLCM features with K-Means clustering and K-Medoids clustering are visualised in Figure 10a and Figure 10b respectively.

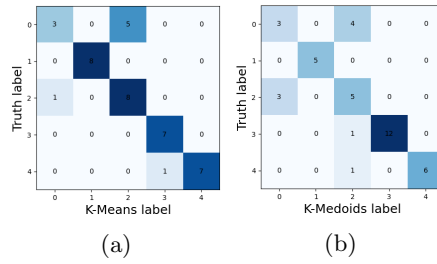


Figure 9: Confusion matrices for CVAE encoded features using K-Means (a) and K-Medoids (b) for different train/test splits

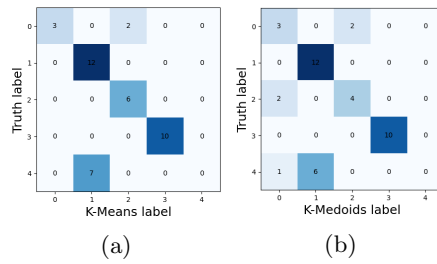


Figure 10: Confusion matrices for comparison between GLCM+K-Means and GLCM+K-Medoids

3.2 Visualisation results

Visualization of the raw data and CVAE encoded features are performed using t-SNE, MDS and LLE methods. Here, the actual data labels are used to map the samples. Initially, the original data $D_{n \times m}$ where $m = 6400$ is transformed and visualised in a 2-dimensional space as it is shown in Figure 11. As illustrated, t-SNE performs reasonable separability between the classes, while there are some overlapping clusters in the case of MDS and LLE.

In order to perform comparison, the second scenario of data visualisation is concerned with transforming the encoded data $D_{n \times 200}$ with t-SNE, MDS and LLE to a 2-dimensional space as seen in Figure 12. Considering the illustration, all three methods showcase an improved performance on the separability of the data into clusters of similarities. However, there are still overlapping between the clusters. Since dimension reduction from 200 encoded features into only two features is a significant reduction of features, no accurate clustering

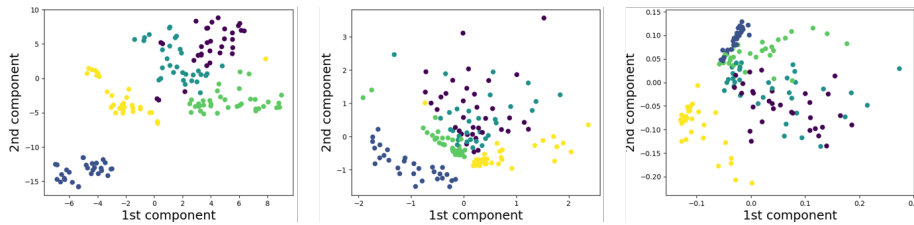


Figure 11: Visualisation of the transformed raw data $D_{n \times 6400}$ using t-SNE, MDS, and LLE

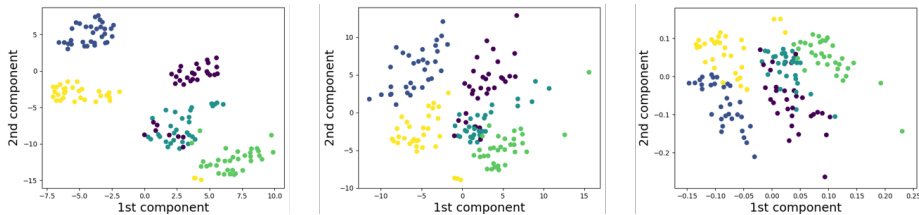


Figure 12: Visualisation of the transformed encoded data $D_{n \times 200}$ using t-SNE, MDS, and LLE

is expected using these two dimensional features. This is tested by applying K-Means and K-Medoids on the two t-SNE features. The average testing accuracies are 42% and 45% for K-Means and K-Medoids respectively. Hence, these manifold learning methods are good for visualisation, but are not necessarily accurate for clustering.

4 Discussion

The confusion matrices for the CVAE-based architecture in Figure 9 reveal that the activities Walking (1) and Jumping (3) are problematic as they are frequently confused. Similarly, the architecture GLCM+K-Means and GLCM+K-Medoids in Figure 10 also show confusion between Walking (1) and Jumping (3). In addition to this, the Standing (5) activity is recognised as Running (2) in nearly all cases as the second architecture suffers from poorer average testing accuracies. As it can be observed from the confusion matrices, the Walking (1), Jumping (3) and Standing (5) classes are seen as problematic. More data can be collected in order to improve the results with a higher number of subjects considering the current small set of data available for this study.

Considering the two proposed architectures, it can be concluded that the encoded data with CVAE is superior in comparison with GLCM features for feature extraction. On the other hand, the GLCM-based model is less complex and it is more easily implemented. The computation time for GLCM is noticeably smaller in comparison with CVAE. The GLCM features are derived from statistical quantification of the texture information in GLCM matrix derived from the 80×80 images as shown in Figure 3. On the other hand, CVAE encoded features are mainly the results of convolutional filtering of the cubic Doppler images of size $2 \times 100 \times 32$. As a whole, the recognition performance for both architectures is reasonable, which can be applied to other unsupervised project scenarios.

The three manifold learning methods considered in this study can be extremely useful for data visualisation problems. As seen in Figure 11, the t-SNE visualisation is better in comparison with MDS and LLE. Since the unsupervised CVAE-based architecture is known to provide a reasonable separation between the clusters, it is compared against the raw data. The results show better separation for all three visualisation techniques seen in 12. It can be concluded that the proposed deep CVAE improves the separability between the classes, which can boost the visualisation results for different manifold learning methods. For high-dimensional data visualisation purposes, the CVAE encoded features can be used prior manifold learning.

5 Conclusion

This work proposes the unsupervised learning approaches for radar Doppler data for daily activity recognition. The results of this work push the applications of Radar Doppler data in healthcare one step forward to practice by enabling the recognition capability without label or with poor label with unsupervised learning. The analysis architecture includes unsupervised feature extraction followed by clustering strategies. Three different categories of unsupervised feature extraction, namely, Convolutional filtering based on deep autoencoders architectures CAE and CVAE, digital image texture analysis based on GLCM and state of the art PCA and SVD techniques, were employed. K-Means and K-Medoids strategies were used for clustering the features. Average testing accuracies reveal the superiority of the CVAE architecture, which achieves $82.5\% \pm 2.73$ and $84\% \pm 5.38$ for K-Means and K-Medoids respectively. In addition, GLCM shows a reasonable performance considering the unsupervised scenario with $77.5\% \pm 0$ and $72.5\% \pm 0$ average testing accuracy for K-Means and K-Medoids respectively. Both architectures are superior when compared with CAE, PCA, and SVD with more than 20% average testing accuracy.

Three manifold learning methods for high-dimensional data visualisation are considered in this study - t-Distributed Stochastic Neighbour Embedding, Multidimensional Scaling and Locally-Linear Embedding. Visualization of the features using these three methods are compared. The results reveal that the clusters have a better separation with all three methods when the visualisation is performed on the CVAE encoded data. Finally, this project can serve as a reasonable application with two appropriate frameworks for project scenarios with poor labeling for both activity clustering and data visualisation.

Acknowledgment

Yordanka Karayaneva thanks the sponsorship of the Data Driven Research Innovation (DDRI) at Coventry University, United Kingdom.

References

- [1] ONS. 2018. Living longer - Office for National Statistics. Retrieved August 29, 2020
- [2] S.U. Park, J.H. Park, M.A. Al-masni, M.A. Al-antari, Md.Z. Uddin, T.-S. Kim, "A Depth Camera-based Human Activity Recognition via Deep Learning Recurrent Neural Network for Health and Social Care Services" in *Procedia Computer Science*, vol. 100, pp. 78-84 2016.
- [3] K.-T. Song and W.-J. Chen, "Human activity recognition using a mobile camera," 2011 8th International Conference on Ubiquitous Robots and Ambient Intelligence (URAI), Incheon, 2011, pp. 3-8, doi: 10.1109/URAI.2011.6145923.
- [4] A. Jalal, S. Kamal, and D. Kim, "A depth video-based human detection and activity recognition using multi-features and embedded hidden Markov

- models for health care monitoring systems,” *International Journal of Interactive Multimedia and Artificial Intelligence*, vol. 4, no. 4, p. 54, 2017.
- [5] S. Patel, H. Park, P. Bonato, L. Chan, M. Rodgers. ”A review of wearable sensors and systems with application in rehabilitation” *J. Neuroeng. Rehabil*, vol. 9, pp. 1–17, 2012.
- [6] M. Al-khafajiy, T. Baker, C. Chalmers, M. Asim, H. Kolivand, M. Fahim, A. Waraich. Remote health monitoring of elderly through wearable sensors. *Multimed. Tools Appl.* pp. 1–26, 2019.
- [7] J. Liu, J. Sohn, S. Kim. Classification of Daily Activities for the Elderly Using Wearable Sensors. *J. Healthc. Eng.* 2017.
- [8] Z. Wang, Z. Yang, & T. Dong. A Review of Wearable Technologies for Elderly Care that Can Accurately Track Indoor Position, Recognize Physical Activities and Monitor Vital Signs in Real Time. *Sensors (Basel, Switzerland)*, vol. 17 no. 2, pp. 341, 2017. <https://doi.org/10.3390/s17020341>
- [9] J. Heikenfeld, A. Jajack, J. Rogers, P. Gutruf, L. Tian, T. Pan, R. Li, M. Khine, J. Kim, J. Wang, & J. Kim. Wearable sensors: modalities, challenges, and prospects. *Lab on a chip*, vol. 18, no. 2, pp. 217–248, 2018. <https://doi.org/10.1039/c7lc00914c>
- [10] A. Kamisalic, I. Jr. Fister, M. Turkanović, M., & S. Karakatič, ”Sensors and Functionalities of Non-Invasive Wrist-Wearable Devices: A Review”, *Sensors (Basel, Switzerland)*, vol. 18, no. 6, pp. 1714. <https://doi.org/10.3390/s18061714>
- [11] S. Patel, H. Park, P. Bonato, L. Chan, M. Rodgers. ”A review of wearable sensors and systems with application in rehabilitation”, *Journal of NeuroEngineering and Rehabilitation*, vol. 9, no. 1, 2012.
- [12] J. Huberty, D. K. Ehlers, J. Kurka, B. Ainsworth, M. Buman. ”Feasibility of three wearable sensors for 24 hour monitoring in middle-aged women”, *BMC Womens Health*, vol. 30, no. 15, 2015.
- [13] Y. Karayaneva, S. Baker, B. Tan, and Y. Jing. ”Use of low-resolution infrared pixel array for passive human motion movement and recognition”, In *British HCI*, Belfast, Northern Ireland, UK, 2018, pp. 1-5.
- [14] S. Mashiyama, J. Hong, and T. Ohtsuki, ”Activity Recognition Using Low-Resolution Infrared Array Sensor,” in *IEEE ICC 2015 SAC – Communication for E-Health*, London, UK, 2015, pp. 495-500.
- [15] S. Mashiyama, J. Hong, and T. Ohtsuki, ”A fall detection system using low resolution infrared array sensor”, in *IEEE International Symposium on PIMRC*, Washington, DC, USA, 2015, pp. 2109-2113.
- [16] Y. Karayaneva, S. Sharifzadeh, Y. Jing, B. Tan, ”Feature Representation of Low-Resolution Infrared Sensor Data for Activity Recognition”, submitted for *IEEE Sensors*, 2020.

- [17] H. Chen and W. Ye, "Classification of Human Activity Based on Radar Signal Using 1-D Convolutional Neural Network," in *IEEE Geoscience and Remote Sensing Letters*, vol. 17, no. 7, pp. 1178-1182, July 2020, doi: 10.1109/LGRS.2019.2942097.
- [18] Y. He, Y. Yang, Y. Lang, D. Huang, X. Jing and C. Hou, "Deep Learning based Human Activity Classification in Radar Micro-Doppler Image," 2018 15th European Radar Conference (EuRAD), Madrid, 2018, pp. 230-233, doi: 10.23919/EuRAD.2018.8546615.
- [19] Q. Chen, B. Tan, K. Woodbridge, K. Chetty. Doppler Based Detection of Multiple Targets in Passive Wi-Fi Radar Using Underdetermined Blind Source Separation. In *Proceedings of the 2018 IEEE International Conference on Radar (RADAR)*, Brisbane, Australia, 27–30 August 2018; pp. 1–6.
- [20] M. S. Seyfioglu, A. M. Ozbayoglu and S. Z. Gurguz, "Deep convolutional autoencoder for radar-based classification of similar aided and unaided human activities," *IEEE Trans. Aerosp. Electron. Syst.*, vol. 54, no. 4, pp. 1709–1723, 2018.
- [21] W. Li, B. Tan, and R. Piechocki, "Passive radar for opportunistic monitoring in E-health applications", *IEEE J. Transl. Eng. Health Med.*, vol. 6, 2018, Art. no. 2800210, doi: 10.1109/JTEHM.2018.2791609.
- [22] F. Wang, M. Skubic, M. Rantz., and P. E. Cuddihy. Quantitative gait measurement with pulse-Doppler radar for passive in-home gait assessment. *IEEE transactions on bio-medical engineering*, vol. 61, no. 9, pp. 2434–2443, 2014. <https://doi.org/10.1109/TBME.2014.2319333>
- [23] M. Zhao, F. Adib, and D. Katabi, "Emotion recognition using wireless signals," in *Proc. ACM Annu. Int. Conf. Mobile Computing and Networking*, 2016, pp. 95–108.
- [24] W. Li, B. Tan, Y. Xu and R. J. Piechocki, "Log-Likelihood Clustering-Enabled Passive RF Sensing for Residential Activity Recognition," in *IEEE Sensors Journal*, vol. 18, no. 13, pp. 5413-5421, 1 July, 2018, doi: 10.1109/JSEN.2018.2834739.
- [25] G. Diraco, A. Leone, P. Siciliano. A Radar-Based Smart Sensor for Unobtrusive Elderly Monitoring in Ambient Assisted Living Applications. *Biosensors (Basel)*. vol. 7, no.4, Published 2017 Nov 24. doi:10.3390/bios7040055
- [26] F. Fioranelli, M. Ritchie, S. Z. Gurbuz, and H. Griffiths "Feature diversity for optimized human micro-doppler classification using multistatic radar", *IEEE Trans. Aerosp. Electron. Syst.*, vol.53, no.2, pp.640–654, Apr. 2017.
- [27] W. Li, Y. Xu, B. Tan and R. J. Piechocki, "Passive wireless sensing for unsupervised human activity recognition in healthcare," 2017 13th International Wireless Communications and Mobile Computing Conference (IWCMC), Valencia, 2017, pp. 1528-1533, doi: 10.1109/IWCMC.2017.7986511.

- [28] Y. Wu, P. Tamayo, K. Zhang "Visualizing and interpreting single-cell gene expression datasets with similarity weighted nonnegative embedding", *Cell Syst.*, vol. 7, pp. 656-666, 2018
- [29] R. L. Thorndike, Who belongs in the family?. *Psychometrika* vol. 18, no.4 pp. 267–276, 1953. <https://doi.org/10.1007/BF02289263>
- [30] C. Yuan and H. Yang, "Research on K-value selection method of K-means clustering algorithm," *Multidisciplinary Scientific Journal*, vol. 2, no. 16, pp. 226-235, 2019.
- [31] P. J. Rousseeuw, "Silhouettes: a graphical aid to the interpretation and validation of cluster analysis", *J Comput Appl Math*, vol. 20, pp 53-65, 1987.
- [32] D. L. Davies and D. W. Bouldin. "A cluster separation measure", *IEEE Transactions on Pattern Analysis and Machine Intelligence*, PAMI-1, no. 2, pp. 224–227, 1979.
- [33] J. Dunn. "Well separated clusters and optimal fuzzy partitions", *Journal of Cybernetics*, vol. 4, pp. 95–104, 1974.
- [34] P. Baldi, "Autoencoders, unsupervised learning, and deep architectures. *Journal of Machine Learning Research*" (Proc. 2011 ICML Workshop on Unsupervised and Transfer Learning), vol. 27, 2012 pp. 37– 50.
- [35] P. Vincent, H. Larochelle, I. Lajoie, Y. Bengio, P.-A. Manzagol, "Stacked denoising autoencoders: Learning useful representations in a deep network with a local denoising criterion", *J Mach Learn Res*, vol. 11, pp. 3371–3408, 2010.
- [36] A. Borghesi, A. Bartolini, M. Lombardi, M. Milano, and L. Benini, "Anomaly detection using autoencoders in high performance computing systems," 2018.
- [37] W. Xu, K. Shawn, G. Wang, "Adversarially approximated autoencoder for image generation and manipulation", *IEEE Transactions on Multimedia*, 2019.
- [38] D. P. Kingma, S. Mohamed, D. J. Rezende, and M. Welling. "Semi-supervised learning with deep generative models". In: *Advances in Neural Information Processing Systems*. pp. 3581–3589, 2014.
- [39] C. Dong, T. Xue and C. Wang, "The Feature Representation Ability of Variational AutoEncoder," 2018 IEEE Third International Conference on Data Science in Cyberspace (DSC), Guangzhou, 2018, pp. 680-684, doi: 10.1109/DSC.2018.00108.
- [40] H. Nishizaki, Data Augmentation and Feature Extraction using Variational Autoencoder for Acoustic Modeling. *AsiaPacific Signal and Information Processing Association Annual Summit and Conference(APSIPAASC)*, 2017, pp. 1222– 1227.

- [41] P. A. Andersen, M. Goodwin, O. C. Granmo. The Dreaming Variational Autoencoder for Reinforcement Learning Environments. In: Max Bramer, Petridis, M. (eds.) *Artificial Intelligence*, vol. 11311, pp. 143–155. Springer, Cham, xxxv edn. (dec 2018). https://doi.org/10.1007/978-3-030-04191-5_11, http://link.springer.com/10.1007/978-3-030-04191-5_11
- [42] D. P. Kingma, M. Welling, "An Introduction to Variational Autoencoders". *Found. Trends Mach. Learn.* vol. 12, pp. 307–392, 2019.
- [43] C. Doersch, "Tutorial on variational autoencoders," arXiv preprint arXiv:1606.05908v2 [stat.ML], 2016.
- [44] Math Works. "Texture Analysis Using the Gray-Level Co-OccurrenceMatrix (GLCM)" - MATLAB & Simulink-MathWorks United Kingdom, 2019. [Online]. Available: <https://uk.mathworks.com/help/images/texture-analysis-using-the-gray-level-co-occurrence-matrix-g lcm.html>
- [45] B. Erol, M. G. Amin, B. Boashash, F. Ahmad, and Y. D. Zhang, "Wide-band radar based fall motion detection for a generic elderly," in *Proceedings of the 2016 50th Asilomar Conference on Signals, Systems and Computers*, Nov 2016 pp. 1768–1772.
- [46] I. T. Jolliffe, *Principal Component Analysis*. New York: Springer-Verlag, 1986.
- [47] Eric W. Weisstein. Singular value decomposition. *MathWorld—A Wolfram Web Resource*, 1999.
- [48] C. Bishop. *Pattern Recognition And Machine Learning*. New York: Springer, 2013, pp.423-430.
- [49] T. Hastie, R. Tibshirani, J. Friedman, "The Elements of Statistical Learning: Data Mining, Inference, and Prediction", 2009, Springer, New York City, USA, pp. 515-518.
- [50] L. J. P. Van der Maaten, & G. E. Hinton, Visualizing high-dimensional data using t-SNE. *J. Mach. Learn. Res.* vol. 9, pp. 2579–2605, 2008.
- [51] J. B. Kruskal. Multidimensional scaling by optimizing goodness of fit to a nonmetric hypothesis. *Psychometrika*, vol. 29, pp. 1–27, 1964.
- [52] J. B. Kruskal. Nonmetric multidimensional scaling: A numerical method. *Psychometrika*, vol. 29, pp. 115–129, 1964.
- [53] T. Hastie, R. Tibshirani, J. Friedman, "The Elements of Statistical Learning: Data Mining, Inference, and Prediction", 2009, Springer, New York City, USA, pp. 570-572.
- [54] S. Roweis and L. K. Saul. Nonlinear dimensionality reduction by locally linear embedding. *Science*, vol. 290 no. 5500, 2000.